

Processing of 4C data from Mahogany Field, Gulf of Mexico

Peter W. Cary and Rodney A. Couzens*

SUMMARY

Two marine 4-C OBC seismic lines were acquired over Mahogany Field in the Gulf of Mexico during the latter part of 1997 and early part of 1998 by Geco-Prakla, and these lines have been made available to the CREWES Project. The primary purpose of acquiring and processing the data was to determine if shear-wave energy could be recorded and imaged from the zone-of-interest below the large salt bodies. Standard time-domain converted-wave processing of the horizontal components of these lines, including provision for anisotropic layering effects and asymmetry between positive and negative offsets, has been performed. The data quality is generally very good, and most of the energy on the inline component appears to be generated by conversion from P to S at the reflector, as observed elsewhere in the world. This report focuses on some of the issues to do with statics, binning and velocities encountered in the standard time-domain processing of this complex structural 4-C data. This analysis uncovers some of the problems that will need to be resolved in the future in order to obtain a higher fidelity image with more sophisticated processing tools such as anisotropic prestack depth migration.

INTRODUCTION

Two high-quality, four-component ocean-bottom cable seismic lines from the Mahogany Field, Gulf of Mexico, have recently been made available to the CREWES Project by Geco-Prakla. Results of the processing of these data sets were presented at the 1998 SEG meeting by Caldwell et al. (1998) and Kendall et al. (1998). The zone-of-interest lies below the Mahogany salt body, which has made it difficult to clearly image the target with regular streamer data. Salt bodies can generate a large amount of mode conversion from P to S energy (Ogilvie and Purnell, 1996), so it is natural to investigate the imaging of all types of waves that are converted from P to S upon transmission through, and reflection from, the salt and sediment boundaries, and recorded on all four components.

Kendall et al. (1998) obtained excellent prestack depth migrated images of the combined hydrophone-vertical geophone data that revealed sub-salt reflections on one of the two lines. Results of this quality have not been obtained from previously acquired streamer data (Caldwell, personal communication), so the quieter recording environment on the sea-floor, and improved multiple attenuation made possible by a dual-cable system, have provided obvious benefits. The processing of the horizontal components of these datasets has been more challenging, so the advantages of the extra two components in the 4C OBC recording are less obvious so far. Changing this perspective will probably depend primarily on whether future improvements in the processing can generate improved images.

* Sensor Geophysical Ltd., Calgary, Alberta

ACQUISITION

Caldwell et al. (1998) provided a complete description of the acquisition, so only the most important aspects are given here. The location of the survey in the Gulf of Mexico is shown in Figure 1.

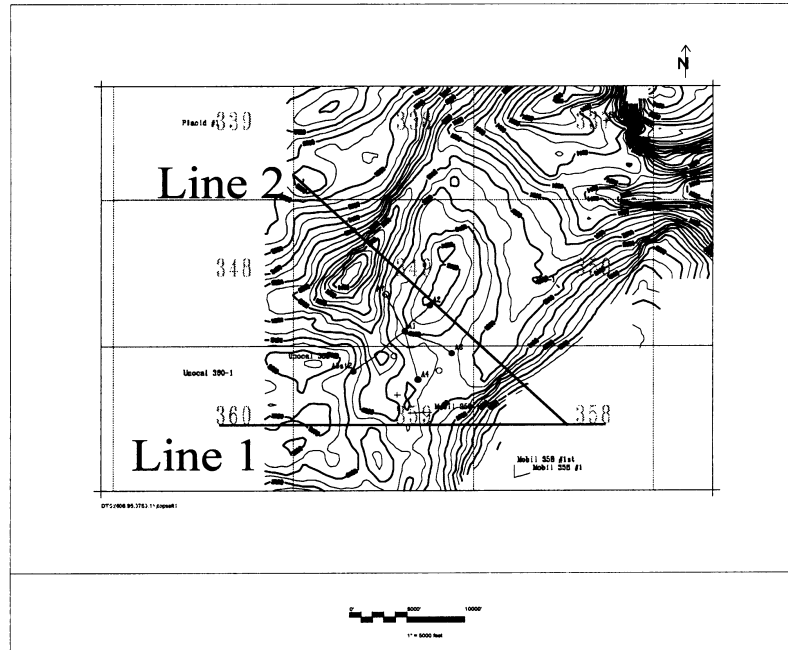


Figure 1. Location of the two 4C OBC lines at Mahogany Field, Gulf of Mexico, showing structural contours to the top of salt and well locations (from Kendall et al., 1998)

The two receiver lines were about 10 km long, which required multiple layouts of the 1500 m-long Geco-Prakla Nessie 4C cable. One line (SS1-4) was oriented east-west, and was thought to be minimally affected by off-line reflections, whereas the other line (SS2-4) was oriented northwest-southeast, and was known from previous surveys to suffer from out-of-plane effects. Nevertheless, Kendall et al. (1998) obtained better images of sub-salt reflectors from the P-P data on Line 2 than on Line 1.

Figure 2 shows a map of the receiver layout for Line 1. Note that the scale of the Y-coordinate is exaggerated with respect to the X-coordinate (the line is actually close to being east-west). Considering that the water-depth is about 120 m, the end-on-end cable layout was remarkably accurate.

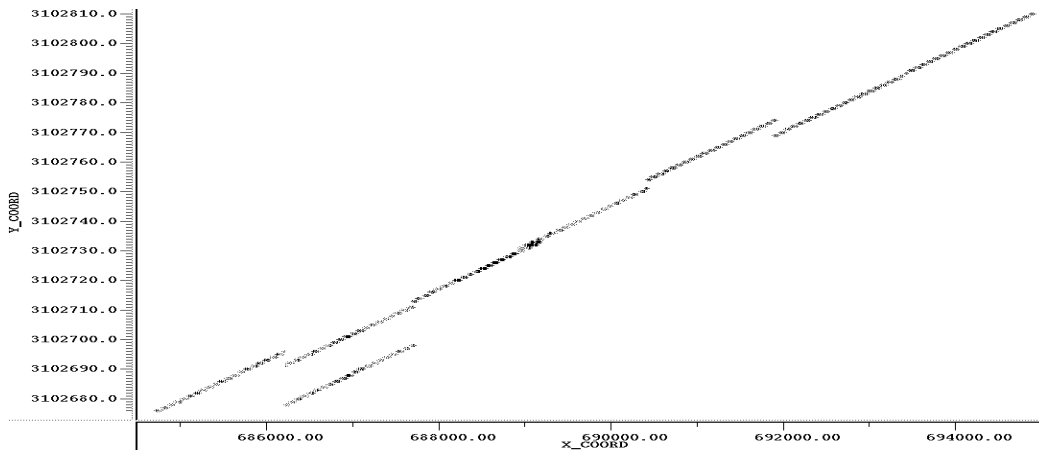


Figure 2. Cable layout for Line SS1-4. Notice that the scale of the y-coordinate is exaggerated compared to the scale of the x-coordinate.

For each cable layout the source boat passed over the cable, shooting every 25 m, with a 10 km run-in and run-out. Within the Nessie 4C cable, 4C receivers are spaced 25 m apart, and additional X-component (inline) geophones were located half-way between each 4C receiver. The additional inline receivers were included in the processing. However, it is doubtful that the additional receivers added to the resolution of the final X-component image, and the processing was complicated by the fact that the geometry of the X-component was different from all other components.

PROCESSING

Line 1

Line 1 was generally the simpler of the two lines to process, so most of the discussion will focus on this line. The data is of good quality for both lines, but the structure just below the ocean-bottom is more complicated for Line 2 than for Line 1, which led to more difficulties in resolving statics. Figure 3 shows the four components of a typical shot gather from Line 1. Notice that the hydrophone component is more ringy than the vertical geophone component. Also note the obvious influence of statics and/or structure on the inline geophone component. The crossline geophone component contains a significant amount of energy, but this component has not been processed at all up to now.

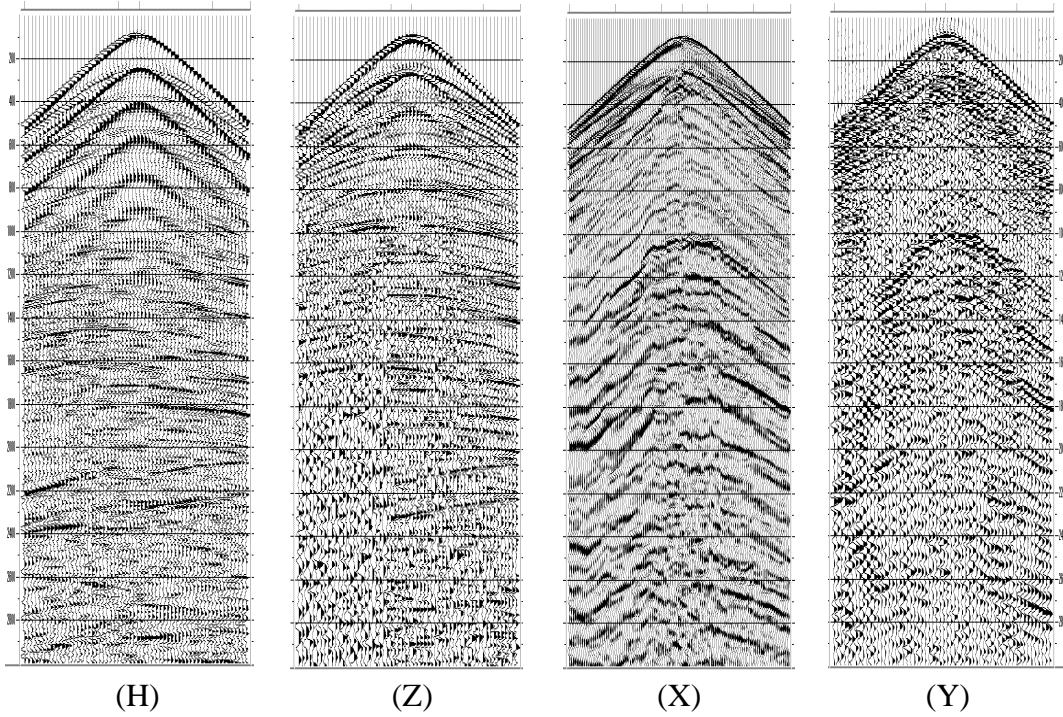


Figure 3. Typical shot gather (1000ms AGC; 770m max. offset) (H) hydrophone (Z) vertical geophone component (X) inline geophone component (Y) crossline geophone component.

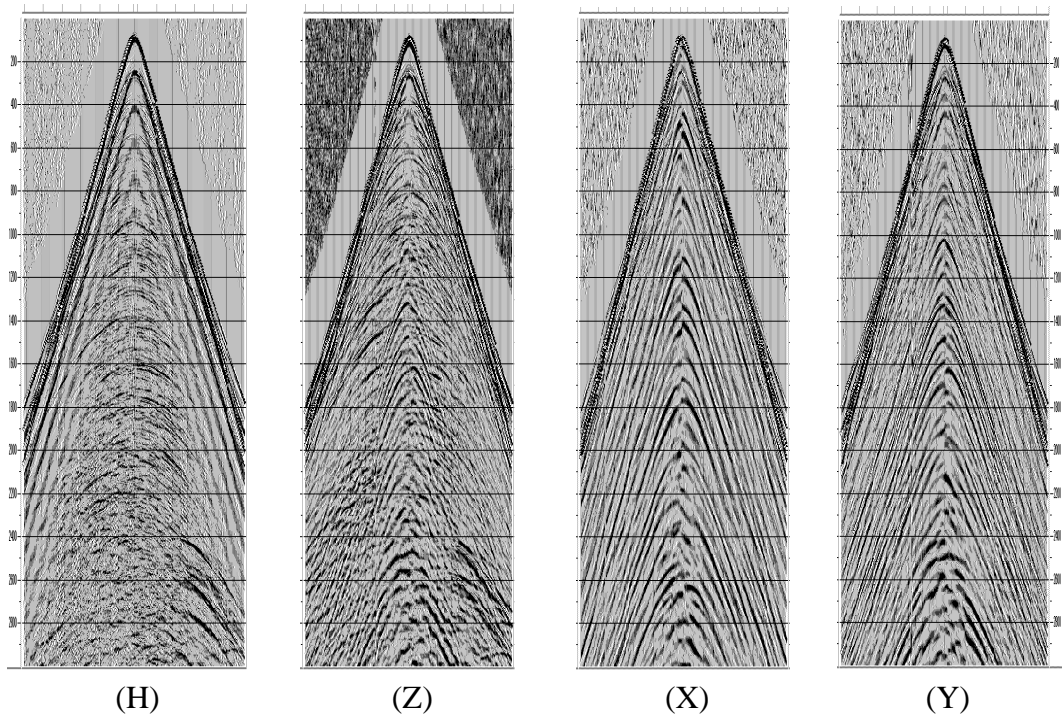


Figure 4. Typical receiver gather (1000ms AGC; 3000m max. offset) (H) hydrophone (Z) vertical geophone (X) inline geophone component (Y) crossline geophone component.

Figure 4 shows four components of a typical receiver gather from Line 1. Notice that statics are now not evident on the X-component. However, there is a significant amount of energy that looks like P-S energy on the vertical component at near offsets. The fact that large statics are evident in the shot domain but not in the receiver domain is clear evidence that the energy on the X-component (at least at shallow times) is predominantly P-S energy that is converted at the reflector, rather than at the sea-floor. Note that AGC has equalized the absolute amplitudes on the X and Y components in Figure 4. Before AGC, the Y-component is weaker than the X component.

Since the main interest is in the converted-wave processing, not a lot of time has been put into the processing of the hydrophone and Z-component data so far, except to get structural information and P-P velocities required for the X-component processing. Figure 5 shows the vertical geophone CMP stack, and Figure 6 shows this stack after poststack time migration. The top of salt is clearly evident at a time of about 3 seconds in the middle of the section. The bottom of salt is less clear than the top, and subsalt reflectors, if there are any, are not obvious.

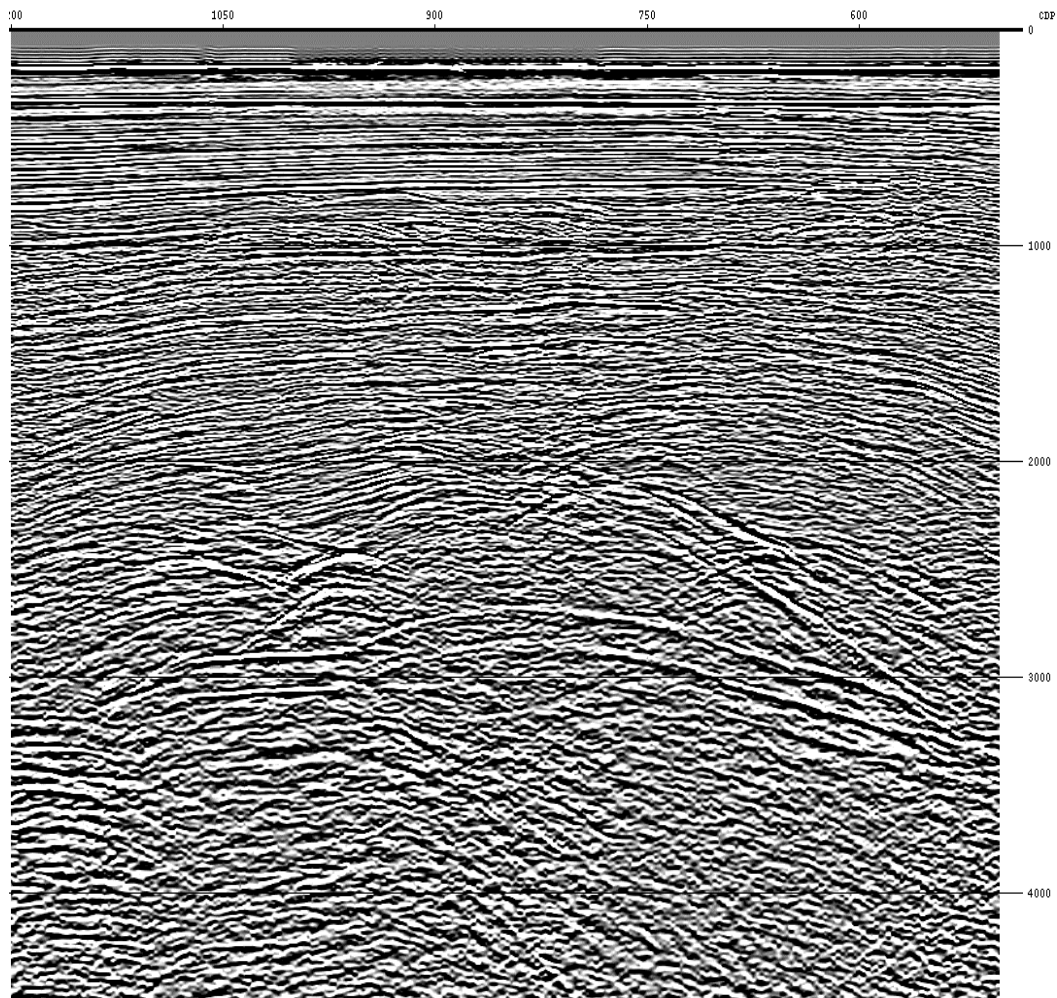


Figure 5. Vertical geophone component CDP stack

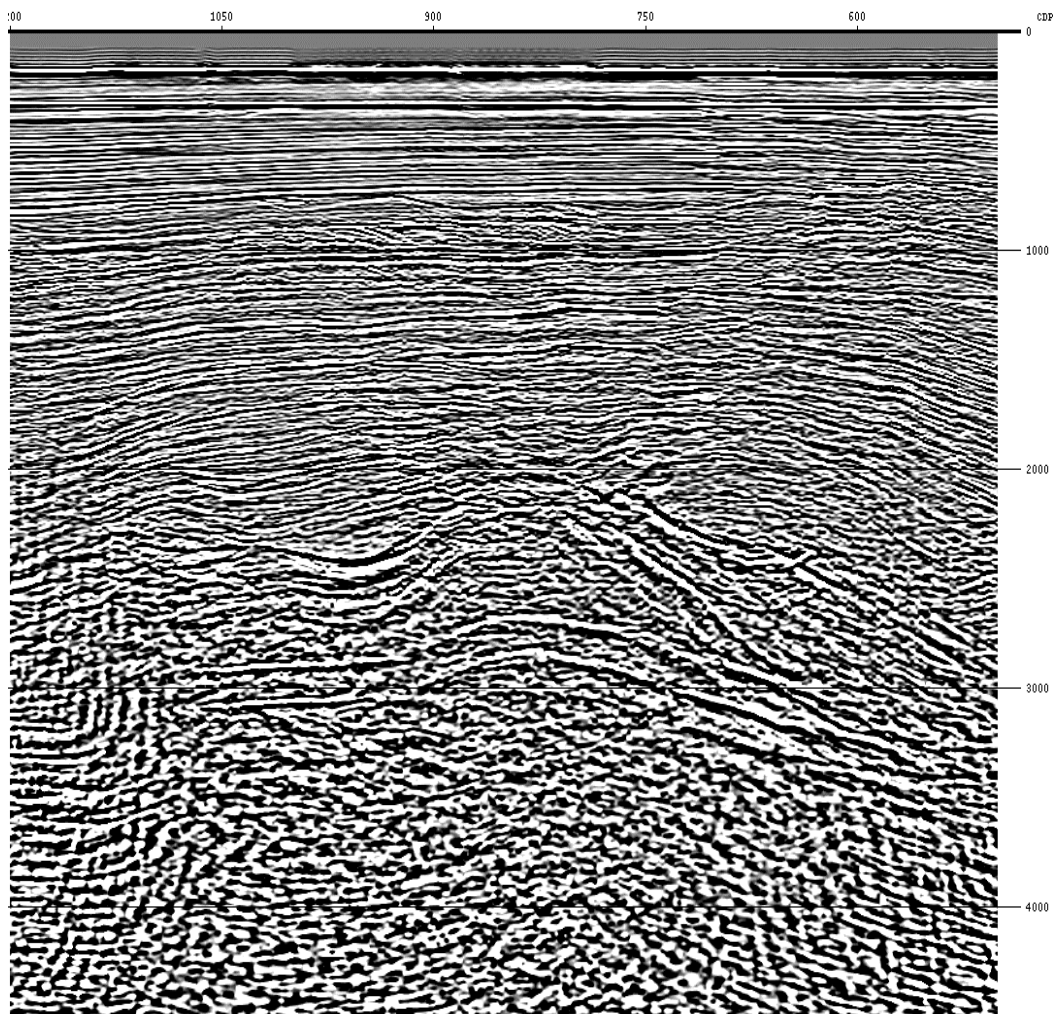


Figure 6. Vertical geophone component poststack time migration.

In processing the X-component data, the first issue to investigate was statics. Unlike 4-C OBC data from other parts of the world such as the North Sea, the data in this particular area unfortunately suffers from relatively large shear statics. Figure 7 shows the common-receiver stack of the X-component of this line with just elevation statics, which effectively bring the shots and receivers to the surface. The comparable common-receiver stack of the Z-component is shown in Figure 8.

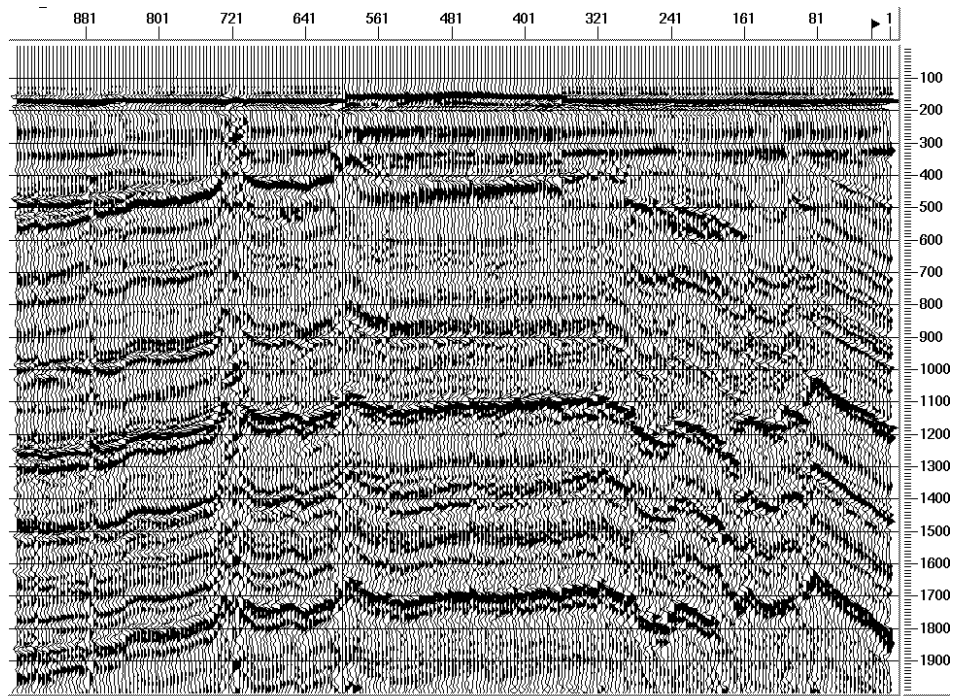


Figure 7. X-component common-receiver stack

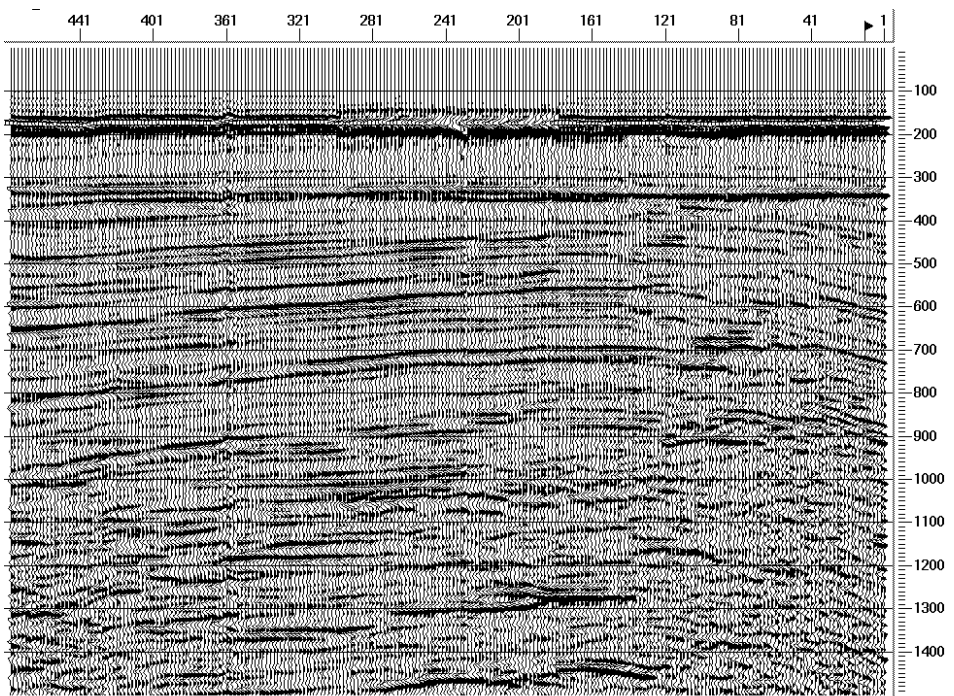


Figure 8. Z-component common-receiver stack

Figure 9 shows a close-up of one part of the X-component common-receiver stack, where one of several high-velocity disturbances below the ocean-bottom on this line is evident. The disturbance has not only caused a static on these receivers, but an obvious scattering effect as well. After static corrections, receivers in the immediate vicinity of this disturbance (and others) were still extremely noisy, and therefore were killed.

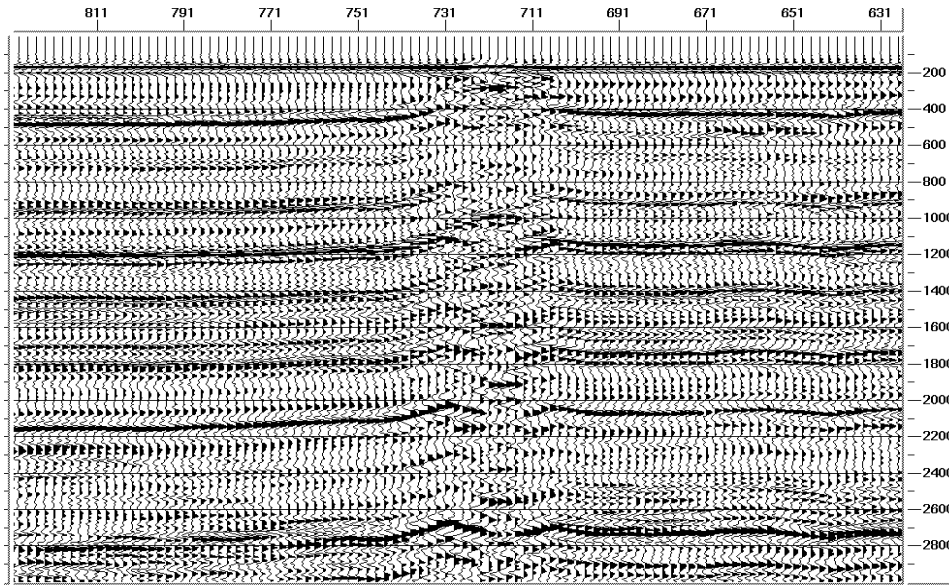


Figure 9. Portion of X-component common-receiver stack with statics

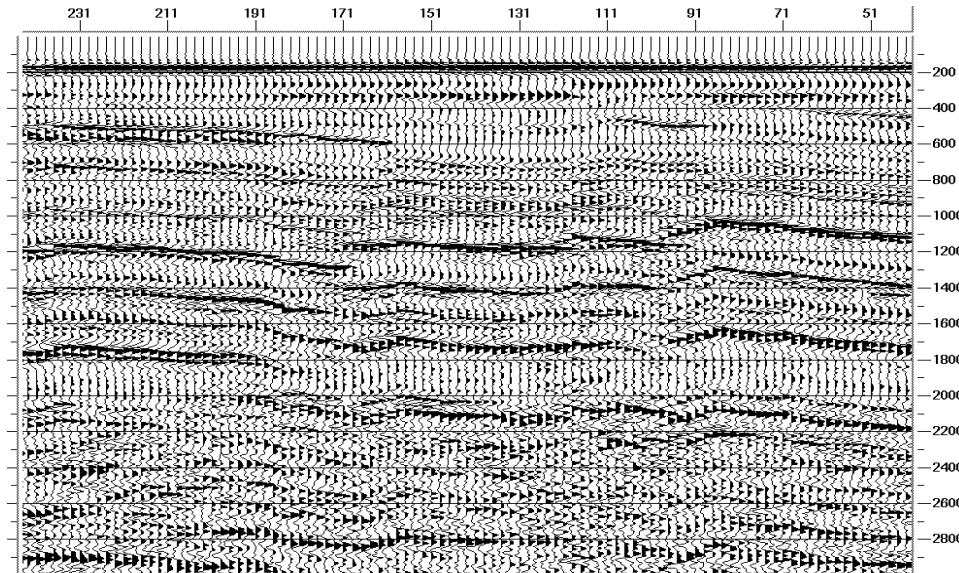


Figure 10. Portion of X-component common-receiver stack with statics and structure

Figure 10 shows another portion of the common-receiver stack where receiver statics are virtually impossible to distinguish from the structural effect of faults coming to the surface. In areas such as this, where short and long-wavelength changes in geologic structure and shear velocity are intermingled, the method of obtaining large converted-wave receiver statics directly from common-receiver stacks (Cary and Eaton, 1993) breaks down. The receiver statics that were applied to the data at this end of the line are therefore poorly determined, both in short- and long-wavelength character.

The final common-receiver stack, with statics solutions applied, is shown in Figure 11. The statics that have been applied to the receivers are the sum of hand statics and automatic residual statics.

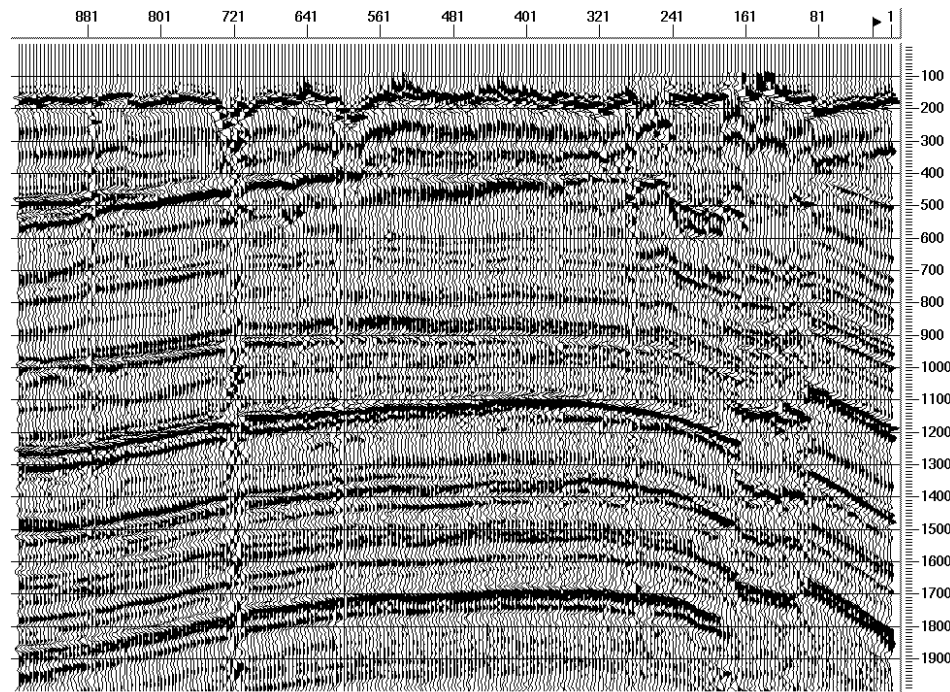


Figure 11. X-component common-receiver stack with statics applied.

The next steps in the processing were the determination of stacking velocities and the velocities to use for depth-variant binning. Thomsen (1998) and others have pointed out the importance of layered anisotropic media on nonhyperbolic moveout and the determination of the conversion point of converted waves. Since a velocity analysis package that includes a quartic (nonhyperbolic) term was not available when this data was processed, standard velocity analysis with hyperbolic moveout was used, so the final mute had to be chosen to be severe enough to eliminate any nonhyperbolic effects at the far offsets. It is doubtful that the inability to flatten the far offsets substantially degraded the quality of the stack, although it would obviously be preferable to include them.

Velocity analysis was initially performed on asymptotically gathered common-conversion-point (CCP) gathers (positive and negative offsets together), with $V_p/V_s = 3.5$, which is a number that was obtained by rough correlation of vertical traveltimes to major reflectors on P-P and P-S stacks. More detailed velocity analysis was performed later in the flow.

An approximate method for CCP binning of converted waves in layered, anisotropic media is to use “effective” V_p/V_s ratios (what Thomsen (1998) calls γ_{eff}) in a depth-variant binning program that is written for isotropic conditions. γ_{eff} is the V_p/V_s ratio that determines the location of the conversion-point, and is a combination of vertical and moveout velocity ratios ($\gamma_{\text{eff}} = \gamma_2^2 / \gamma_0$, where γ_2 is the ratio of P-P and S-S moveout velocities and γ_0 is the ratio of average vertical velocities). Thomsen (1998) gives a method of determining γ_{eff} directly from the data by using measured values of γ_0 , P-P and P-S stacking velocities at corresponding times (his equation 17). This equation was found to be too sensitive to errors in the measured values to be of practical use (unreasonably large positive and negative effective V_p/V_s ratios were obtained). Instead, the best γ_{eff} for each major set of layers in the final stack was chosen by analysing the focusing of dipping events on constant V_p/V_s stacks. This process is fairly sensitive to V_p/V_s when analysing dipping events, but is ineffective for flat events. A more accurate, quantitative method of determining γ_{eff} would be very useful, if it existed. Figure 12 shows an example of how one portion of the depth-variant stack changes with γ_{eff} . The values of γ_{eff} used for binning the data were consistently lower than γ_0 , the values obtained by correlating vertical traveltimes. Therefore, conversion points were located closer to the shots in this anisotropic analysis than they would have been with a purely isotropic analysis based on vertical traveltimes. For example, for the layers immediately above the salt, $\gamma_{\text{eff}} = 2.2$ was used for binning based on the focusing of the depth-variant stacks, whereas vertical traveltimes indicated that $\gamma_0 \cong 2.8$ in these layers. For an offset of 5000m, the difference in asymptotic binning location for these two values of V_p/V_s is about 250m, which is certainly significant.

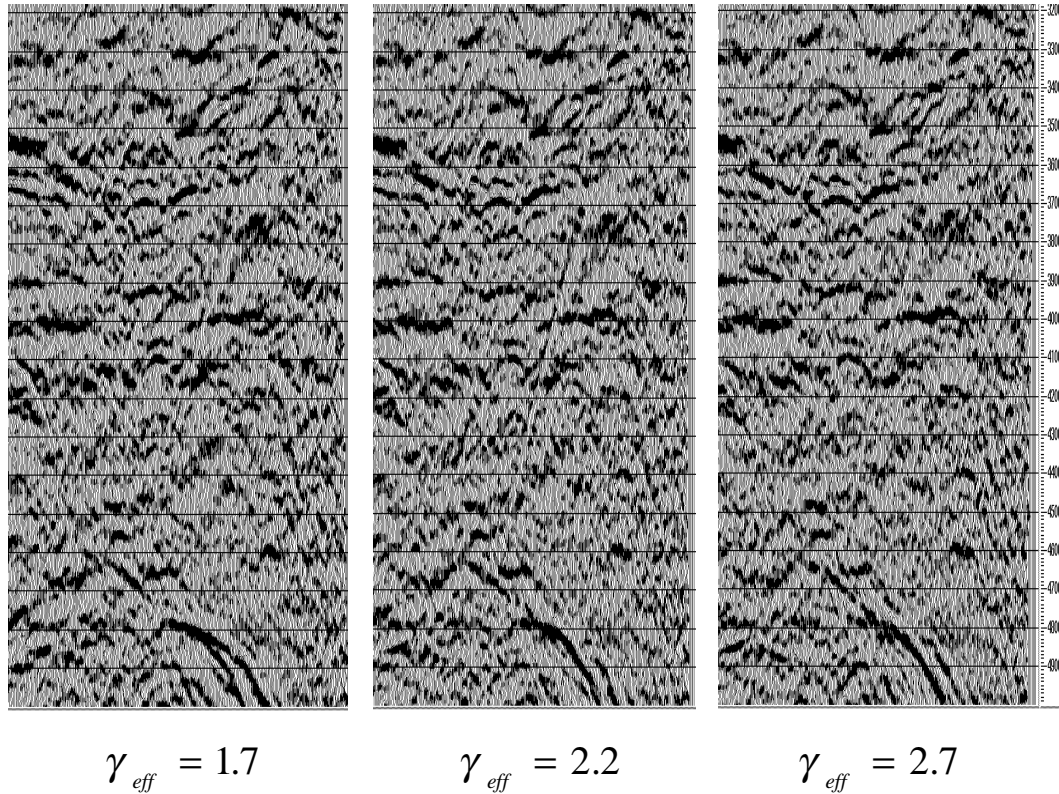


Figure 12. Constant Vp/Vs depth-variant stacks illustrating how changes in binning affects the focusing of dipping events.

The processing of marine converted-wave data that has been acquired in the vicinity of gas clouds has clearly demonstrated that large differences in stacking velocities can occur between negative offsets and positive offsets because of the asymmetric effect of lateral velocity variations on converted-wave raypaths (Thomsen, 1998). Although gas clouds are not present in this area, separate velocity analysis was performed on positive and negative offsets since lateral velocity variations may still influence positive and negative offsets differently.

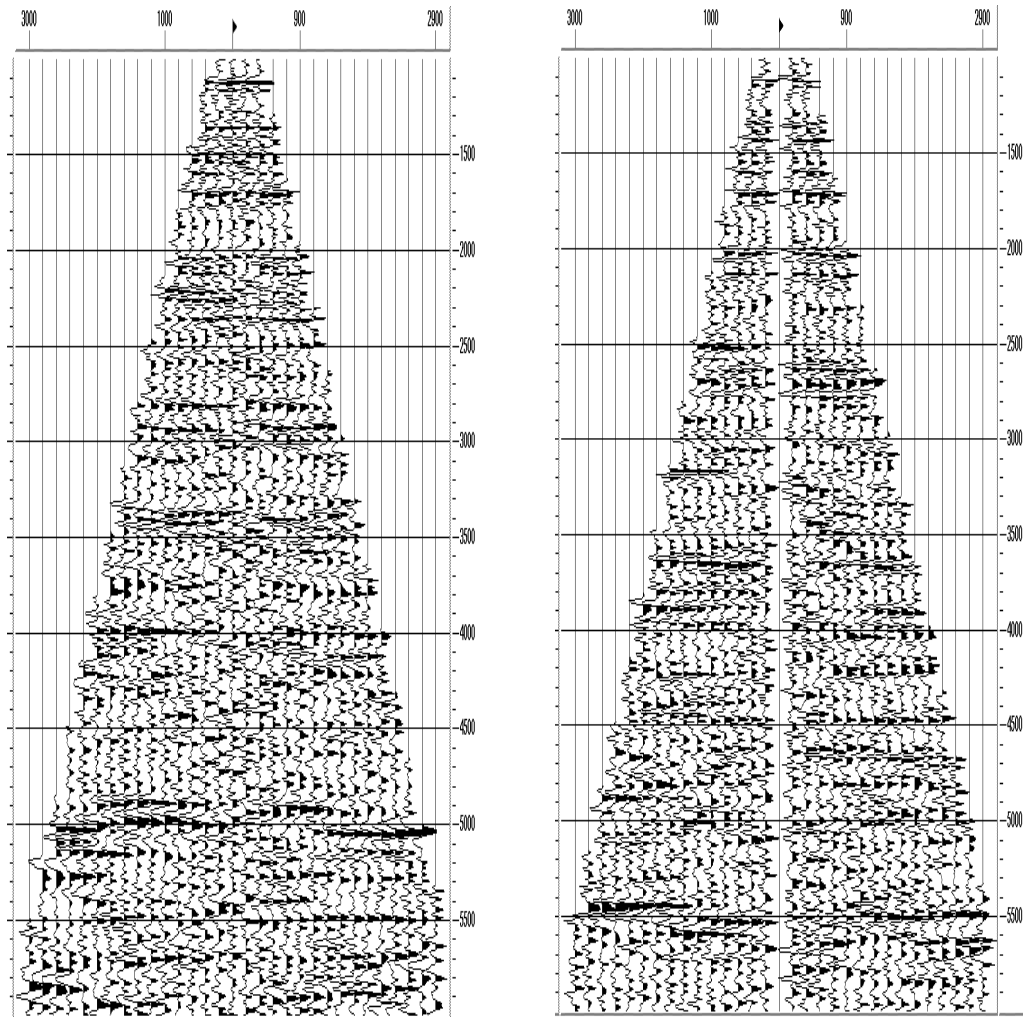


Figure 13. Typical common-offset stacks (X-component) illustrating different character of reflections on positive and negative offsets.

Although no obvious instances of velocity differences between positive and negative offsets were observed, there are many instances of differences in character of the reflections on the two offsets. For example, Figure 13 shows two typical X-component common-offset stacks after depth-variant binning. At both locations, reflections at early times are similar in character on the positive and negative offsets, but at later times differences such as hyperbolic versus nonhyperbolic moveout and even apparent polarity or phase changes from one side of the gather to the other occur. The reason, or reasons, for these differences in character is presently being investigated, but there are many possibilities: P-P reflections, multiples, off-line

energy, multimode energy (e.g. PS-S, PS-PS raypaths), inaccurate binning and/or velocities, statics, raybending, anisotropy, etc.

Despite the differences between positive and negative offsets, stacking velocity analysis was relatively straightforward for reflections above the salt. Extremely low stacking velocities (less than 800 m/s) were required to flatten reflections in the shallowest part of the section (first 2 seconds). Difficulties in imaging reflections below the top of salt were expected due to multiple modes passing through, and reflecting from, the salt/sediment boundaries (Ogilvie and Purnell, 1996). Some evidence for these multiple modes was observed during velocity analysis, by the fact that velocities often appeared to split into two or three trends below the top of salt reflection, as illustrated in Figure 14. Generally velocity analysis became very difficult to pick reliably below the top of salt, especially since no well log information was available to guide the picking.

Converted-wave dip moveout was performed on the data, but did not appreciably improve the quality of the final stack, nor did velocities appear to change after DMO. As expected from the differences in character between positive and negative offsets on the common-offset stacks, differences in the DMO stacks for the positive and negative offsets also occurs. A particularly interesting difference that occurs between positive and negative-offset DMO stacks (and stacks without DMO) is the one-sided manner in which diffractions are imaged. Figure 15 shows a portion of the positive-offset DMO stack that shows diffracted energy dipping predominantly to the west (sources are east of receivers in Figure 15). Figure 16 shows the same portion of the negative-offset DMO stack that shows diffracted energy dipping predominantly to the east (sources are to west of receivers in Figure 16). This unexpected difference between positive- and negative-offset stacks on the X-component data is in need of explanation. The Z-component positive- and negative-offset stacks shown in Figures 17 and 18 do not exhibit the same differences in character of the diffractions.

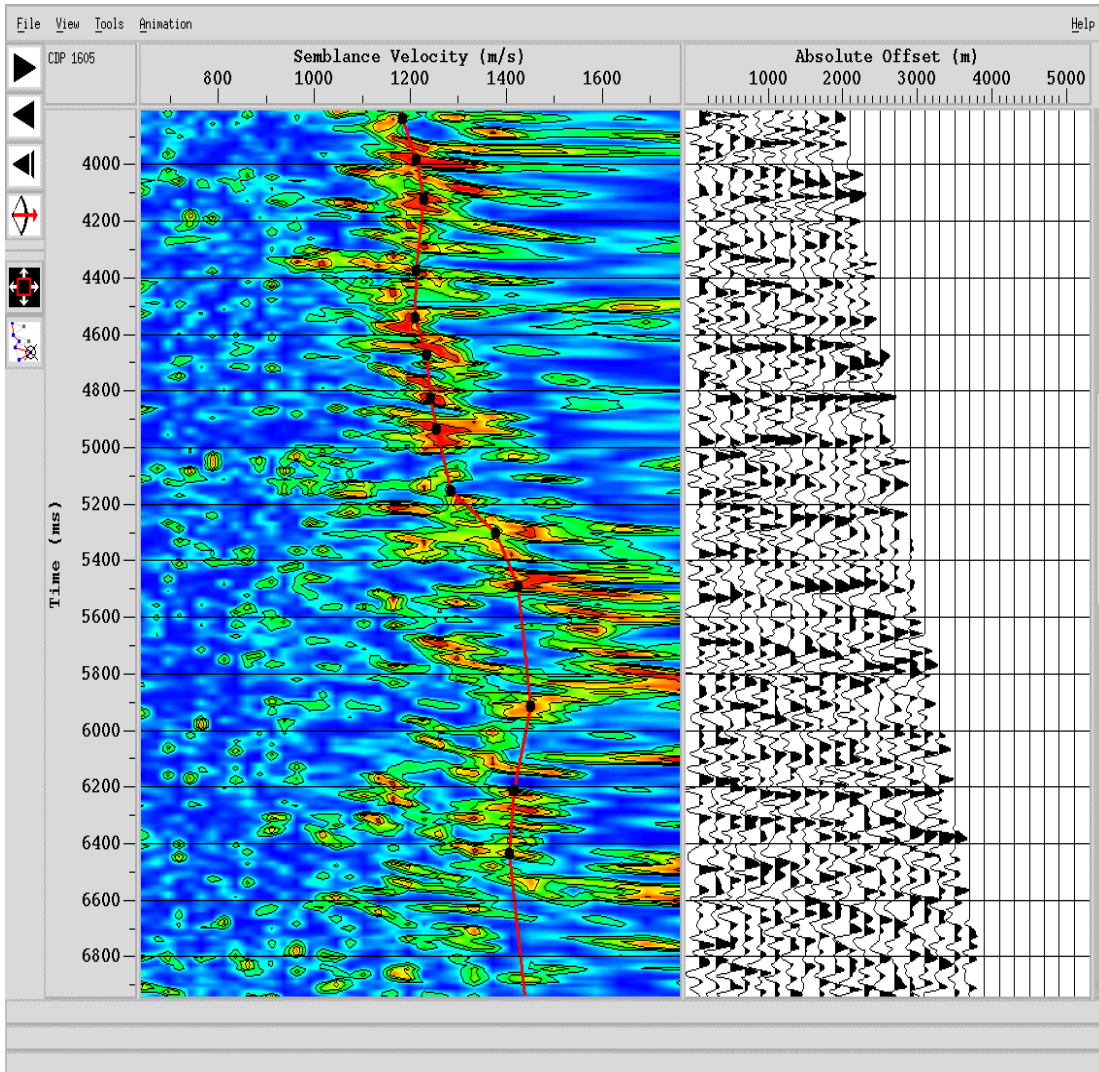


Figure 14. Typical velocity analysis panel from X-component data showing trend of velocities above, through and below salt.

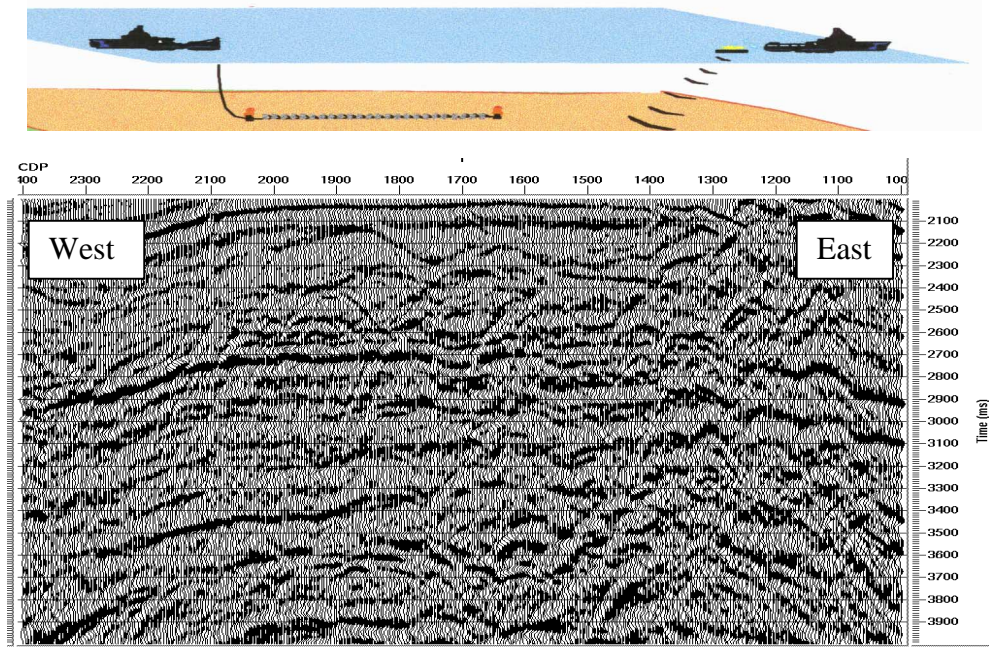


Figure 15. Positive-offset DMO stack showing predominantly west-dipping diffractions.

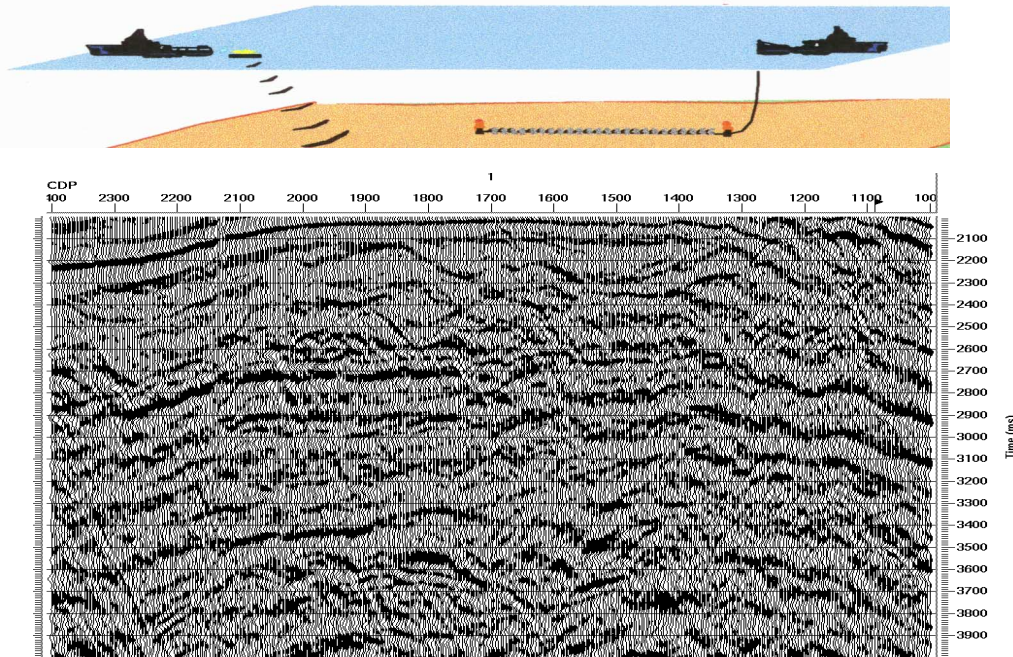


Figure 16. Negative-offset DMO stack showing predominantly east-dipping diffractions.

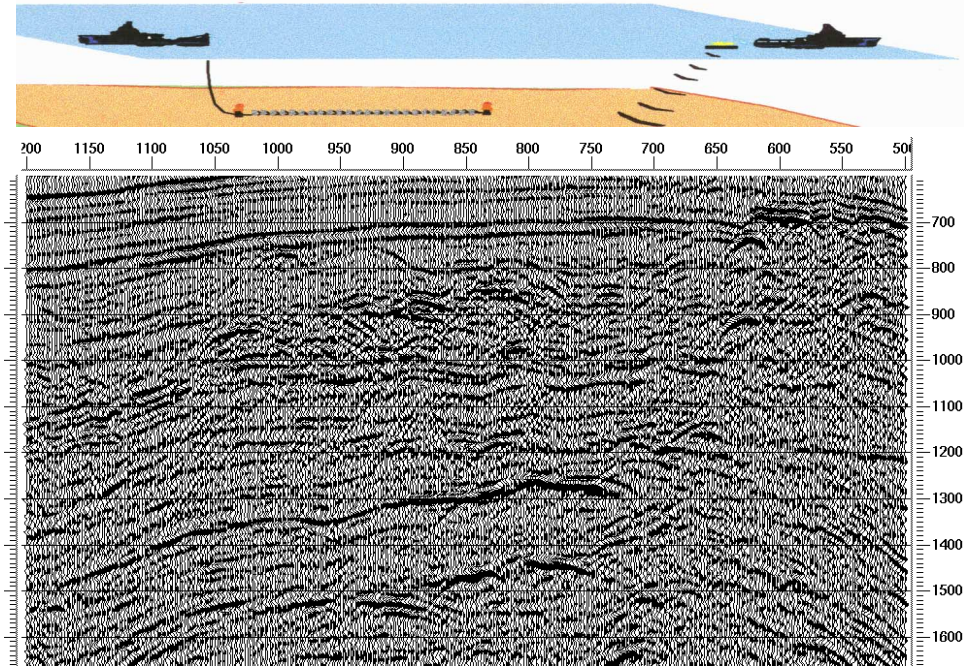


Figure 17. Positive-offset CDP stack of vertical geophone component

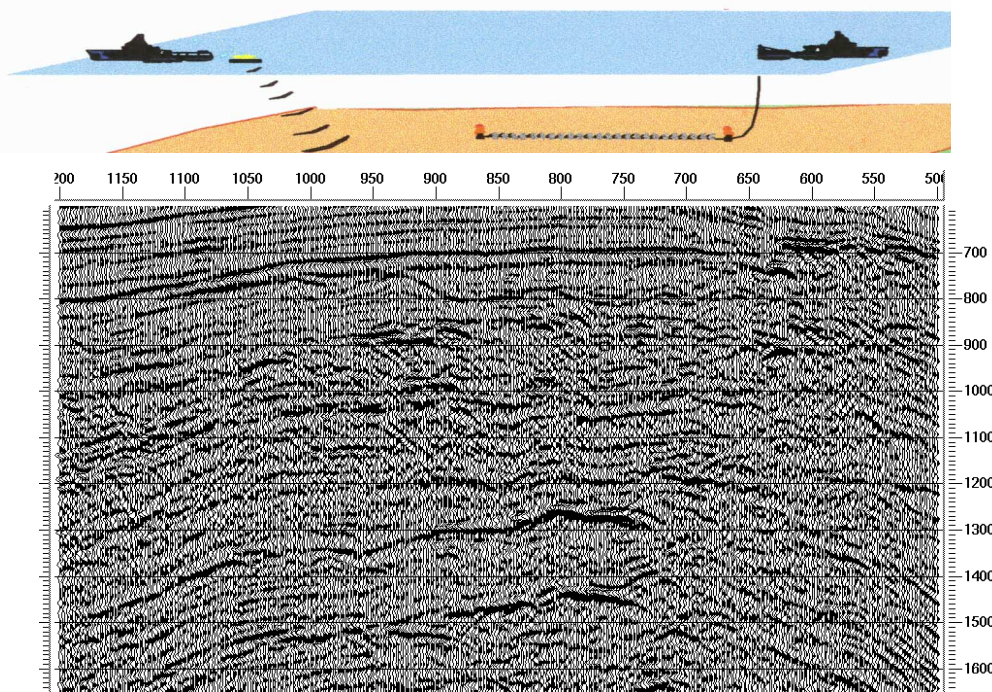


Figure 18. Negative-offset CDP stack of vertical geophone component

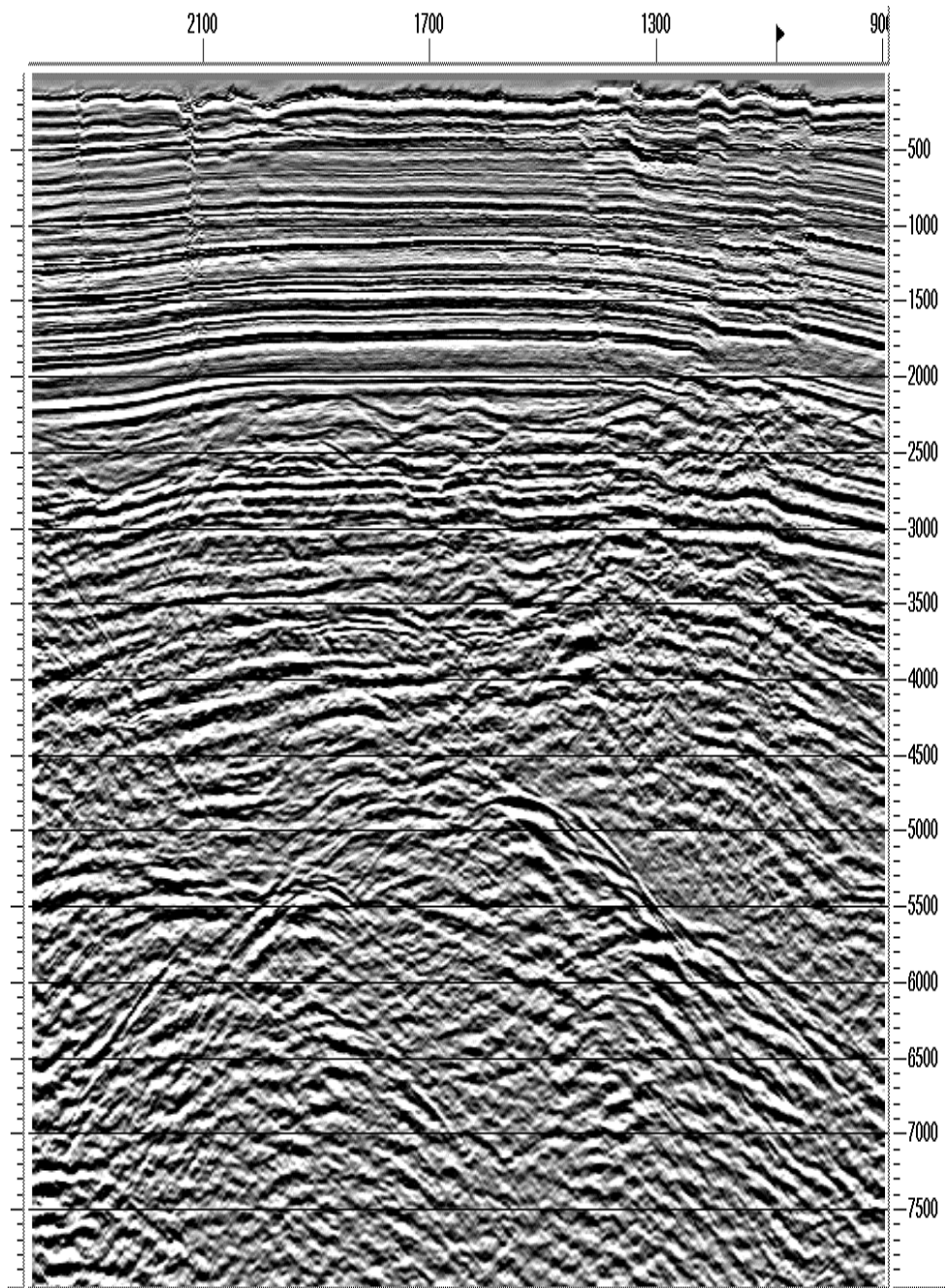


Figure 19. P-S DMO stack (all offsets) of X-component data

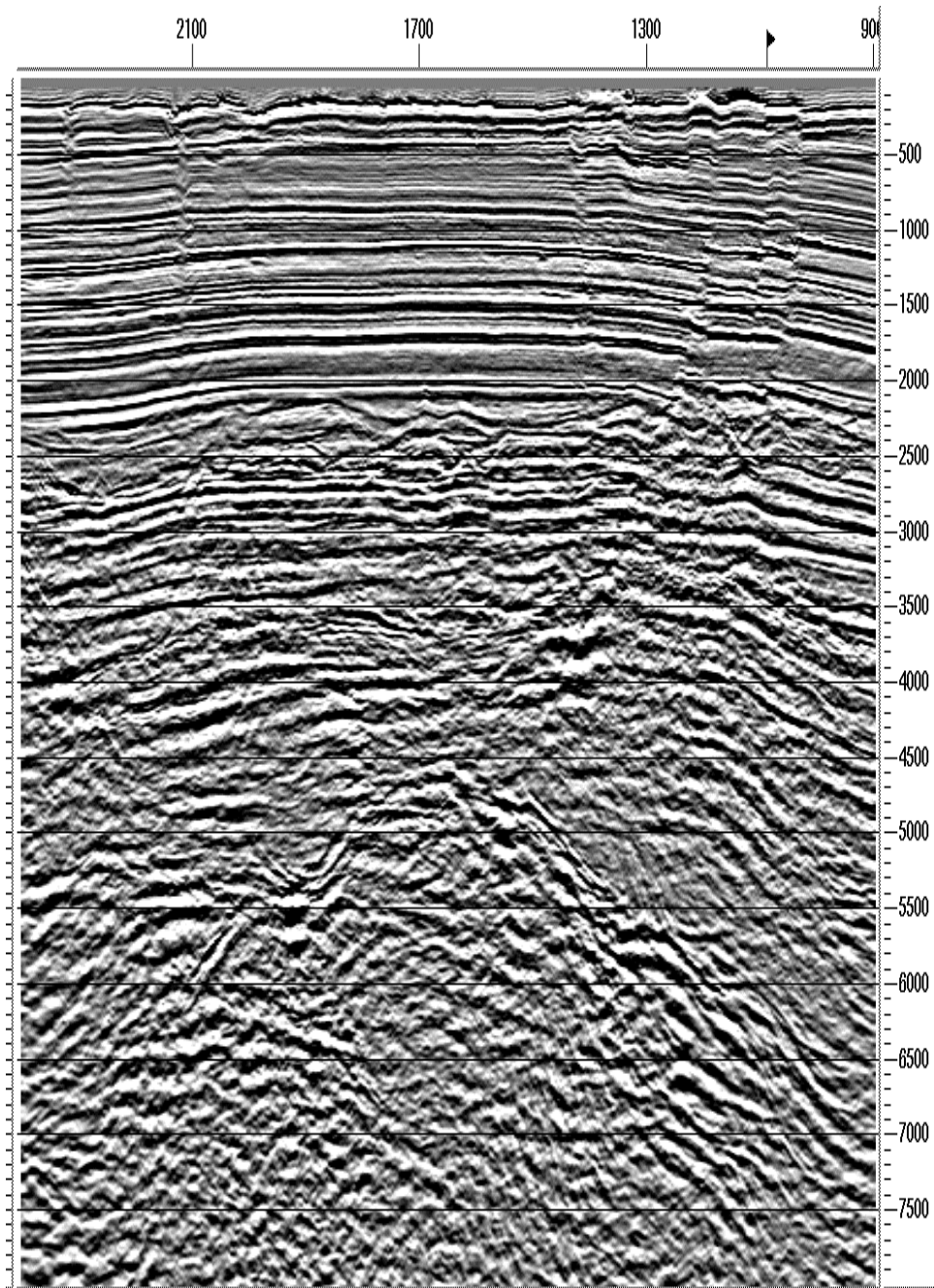


Figure 20. Poststack time migrated DMO stack of X-component data

Despite the obvious differences between the two stacks, the positive and negative offsets were combined to produce the final full-offset DMO stack, as shown in Figure 19. This stack was then poststack time migrated (Figure 20) with 80% of the smoothed stacking velocities. In Figure 20, the top of salt is clearly visible, the bottom of salt is less well defined, and it is difficult to have any confidence in the identification of any subsalt reflectors.

Line 2

The processing of Line 2 was similar to Line 1 in most respects, but also offered some additional challenges. The CMP stack of the Z-component is shown in Figure 21. As previously noted, more off-line energy was expected on Line 2 compared to Line 1, which makes the poststack migration in Figure 22 less likely to be correct.

The depth-variant stack of the X-component is shown in Figure 23, and the poststack time migration is shown in Figure 24. Some obvious structural differences between the vertical and horizontal components occur on these two sections. One particular section of the top of salt is almost flat on the X-component, but is dipping on the Z-component (the reflection between CDP 600 and CDP 800, from 2000ms to 2200ms on the Z-component stack), which may be indicative of large velocity differences between the P-velocities and S-velocities, or else very different traveltimes to off-line reflectors occurring for the two wave types. In addition, structural differences occur in the shallowest part of the section, which are indicative of unresolved, long-wavelength shear statics. Similar long-wavelength structural variations do not occur on the Z-component section. Figure 25 shows the X-component receiver stack for the line. Faulting occurs in the shallow part of the section to a more severe degree than on Line 1, so it is even less likely that near-surface shear-velocity variations have been isolated in the receiver stack than on Line 1. It is not possible to resolve the receiver statics with confidence in several parts of the stack. The structural variations that remain in the stack after static correction are therefore very much a personal interpretation. Perhaps replacing static corrections with detailed depth migration in these shallow parts of the P-S stack, and forcing the P-S depth migrated stack to be structurally similar to the P-P depth-migrated stack, would lead to a more credible result than with poorly constrained statics from receiver stacks.

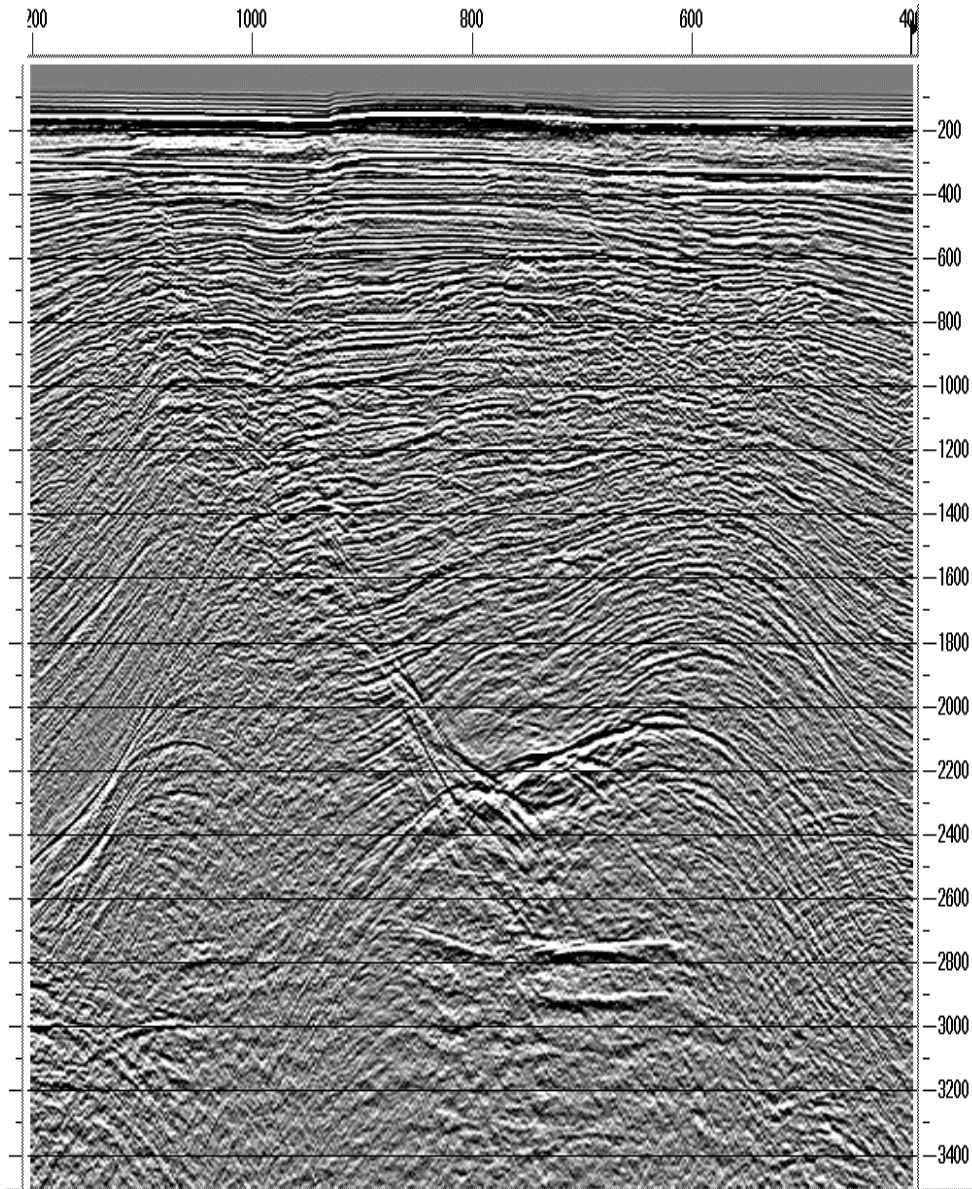


Figure 21. CDP Stack of vertical geophone component from Line 2

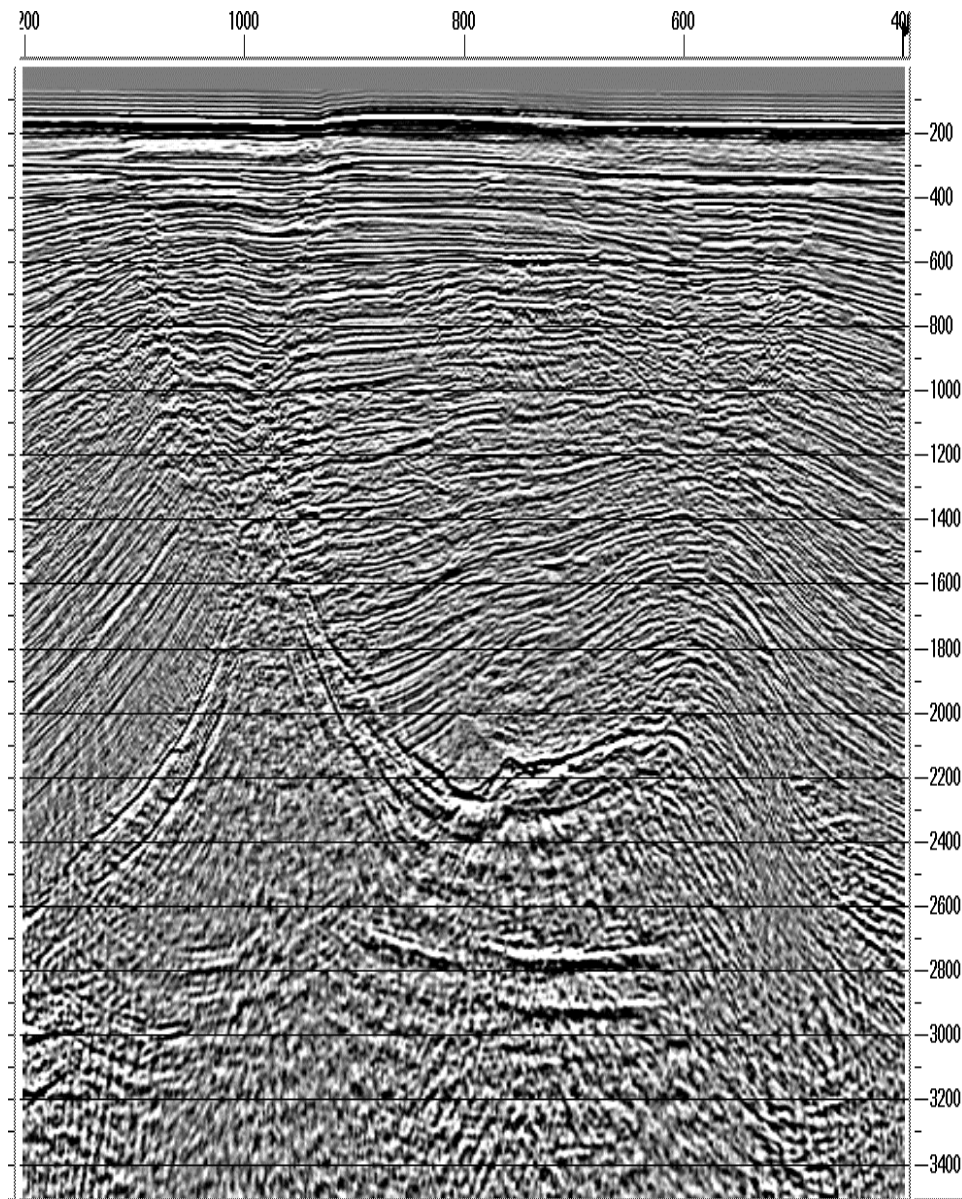


Figure 22. Post-stack time migrated stack of vertical geophone component from Line 2

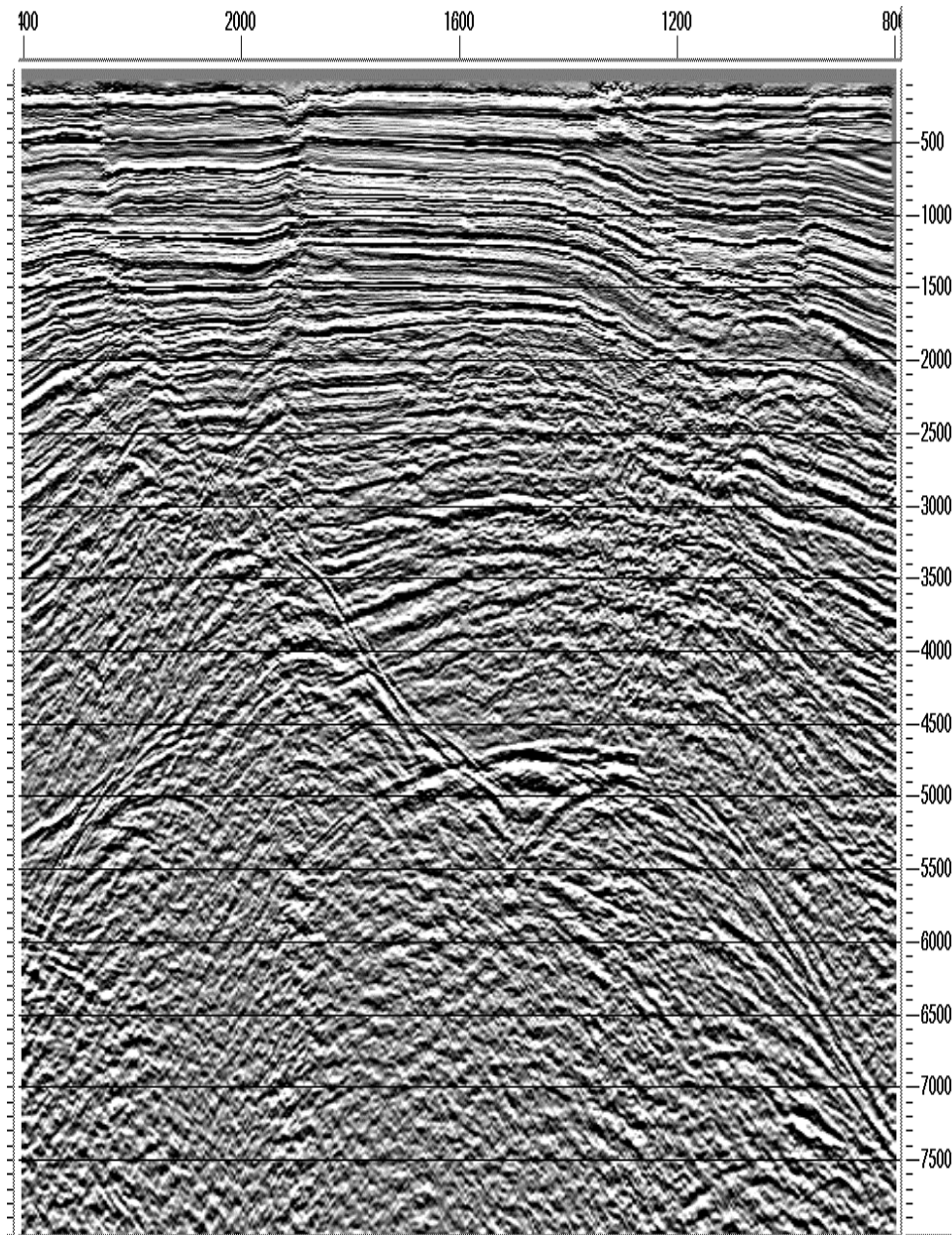


Figure 23. Depth-variant CCP stack of X-component data from Line 2

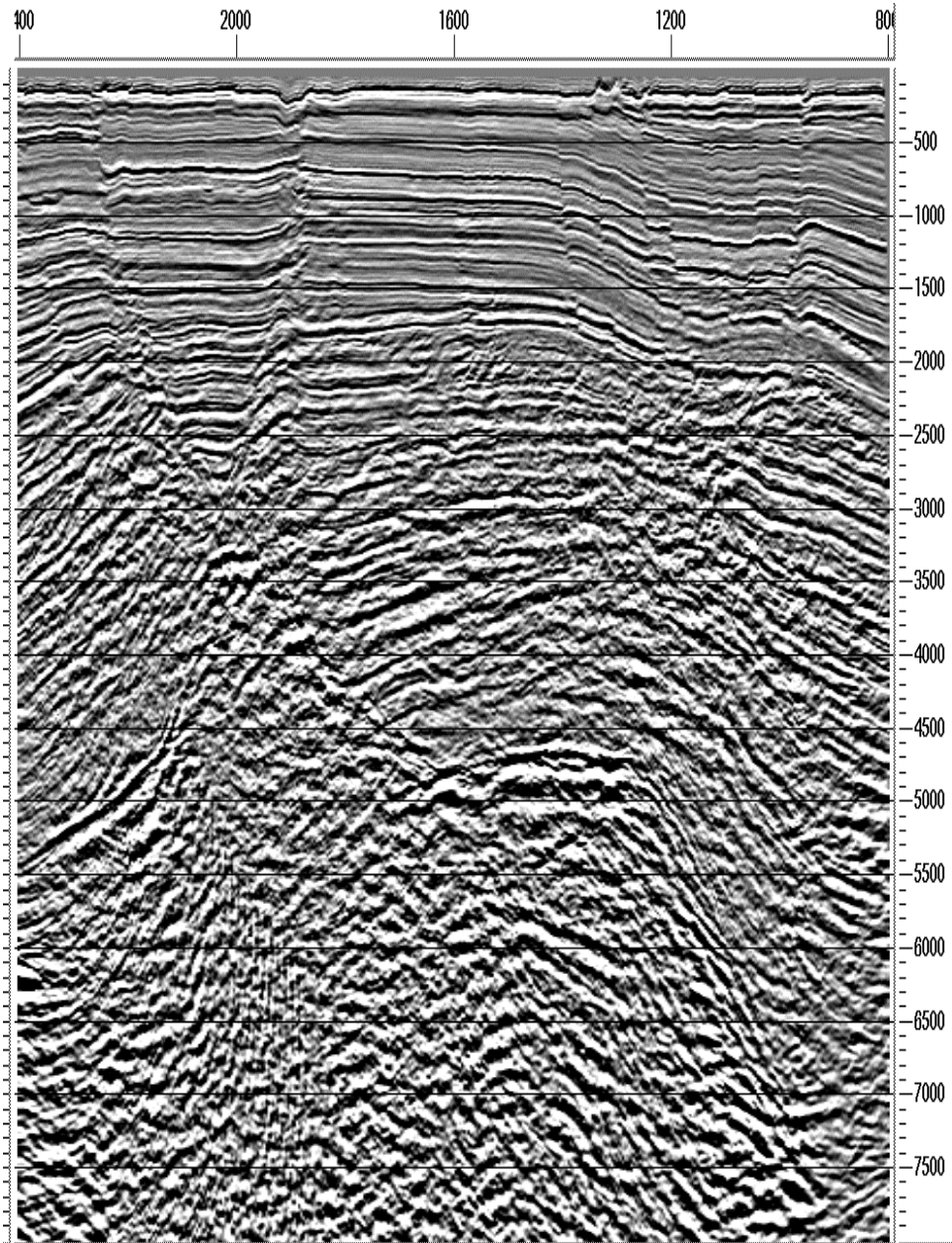


Figure 24. Post-stack time migration of depth-variant CCP stack of X-component from Line 2

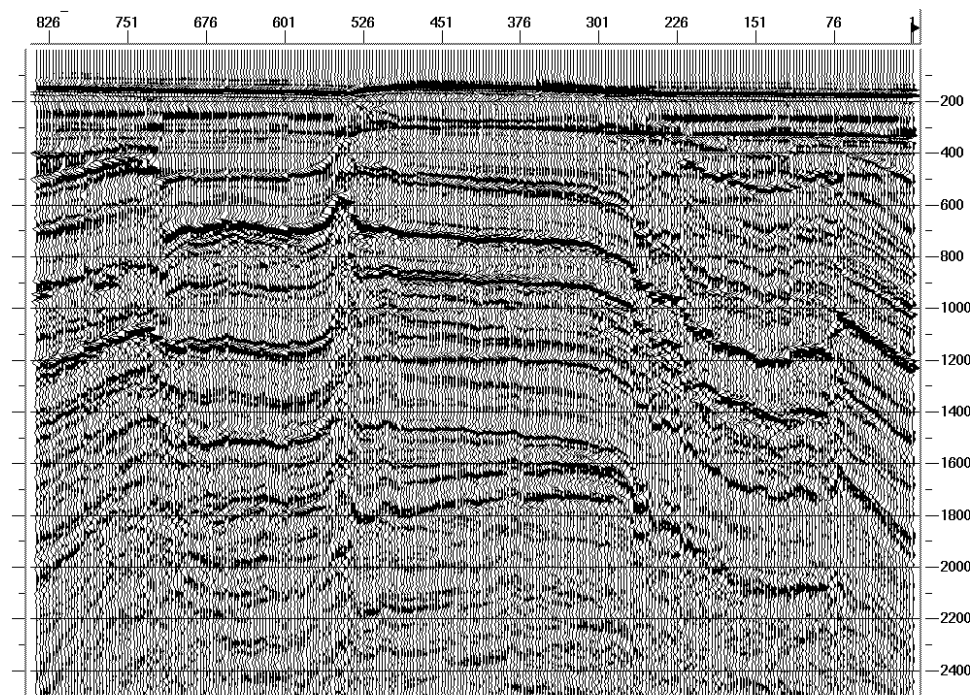


Figure 25. Common-receiver stack of X-component data from Line 2

CONCLUSIONS

These two 4C lines have uncovered a number of problems in the processing of the X-component data:

- 1) When significant structural variations and shear-velocity variations coincide, we presently have no reliable method of separating the two.
- 2) Differences between positive and negative offsets on common-offset stacks are larger than expected (apparent polarity changes, etc.).
- 3) Differences between positive and negative offsets on stacks are larger than expected (diffractions are one-sided).
- 4) A more accurate method of estimating the effective V_p/V_s ratio for binning is needed for taking into account anisotropic layered media, especially for flat reflectors.
- 5) Attenuation of the multiples in the water column is needed, which might resolve some of the confusing differences pointed out in 2).

- 6) Wavefield separation would undoubtedly make the analysis of the data much simpler and easier (not only P/S separation, but separation of multimodes from simple P-S reflections).

Before pursuing ambitious projects like 3-D anisotropic prestack depth migration, which this type of data ultimately requires for accurate imaging, it is probably worthwhile to try to resolve some of the problems listed above first.

ACKNOWLEDGEMENTS

We would like to thank Geco-Prakla, especially Jack Caldwell, for permission to release these datasets to the CREWES Project. We would also like to thank Jack Caldwell and Gerry Beaudoin (Amoco) for valuable discussions about the processing.

REFERENCES

- Caldwell, J., Kristiansen, P., Beaudoin, G., Tollestrup, K., Siddiqui, S., Wyatt, K., Camp, W. and Raney, G., 1998, Marine 4-component seismic test, Gulf of Mexico: subsalt imaging at Mahogany Field: 67th Ann. Internat. Mtg. Soc. Expl. Geophys. Expanded Abstracts, 2091-9092.
- Cary, P.W. and Eaton, D.W.S., 1993, A simple method for resolving large converted-wave (P-SV) statics, *Geophysics*, 429-433.
- Kendall, R.R., Gray, S.H. and Murphy, G., 1998, Subsalt imaging using prestack depth migration of converted waves: Mahogany Field, Gulf of Mexico: 67th Ann. Internat. Mtg. Soc. Expl. Geophys. Expanded Abstracts, 2052-2055.
- Thomsen, L., 1998, Converted-wave reflection seismology over anisotropic, inhomogeneous media, 67th Ann. Internat. Mtg. Soc. Expl. Geophys. Expanded Abstracts, 2048-2051.
- Ogilvie, J.S. and Purnell, G.W., 1996, Effects of salt related mode conversions on subsalt prospecting, *Geophysics*, **61**, 331-348.